CMST 28(2) 61–75 (2022) DOI:10.12921/cmst.2022.0000015

Rise of the Poisson's Ratio in f.c.c. Hard Sphere Crystals with the Narrowest Orthogonal Nanochannels Filled by Hard Spheres of Another Diameter

J.W. Narojczyk[1*], **K.V. Tretiakov**[1,2†], **K.W. Wojciechowski**[1,2‡]

[1] *Polish Academy of Sciences*
Institute of Molecular Physics
M. Smoluchowskiego 17, 60-179 Poznań, Poland

[2] *Calisia University – Kalisz*
Nowy Świat 4, 62-800 Kalisz, Poland

[*] *E-mail: narojczyk@ifmpan.poznan.pl*
[†] *E-mail: tretiakov@ifmpan.poznan.pl*
[‡] *E-mail: kww@ifmpan.poznan.pl*

Received: 13 June 2022; revised: 20 June 2022; accepted: 21 June 2022; published online: 30 June 2022

Abstract: Auxetic materials, i.e. materials exhibiting negative Poisson's ratio, stand to answer the demand for novel materials with unique and application-tailored properties. The vast range of potential applications motivates researchers to search for new materials with such properties, or to look for ways to modify the properties of existing materials. The study of systems with structural inclusions falls into the latter category. This work reports numerical investigations of elastic properties of hard sphere f.c.c. crystal. The investigations have been focused on Monte Carlo simulations of systems with arrays of inclusions filled by hard spheres of different diameter, resulting in binary systems, i.e. systems composed of two kinds of particles that differ only in size. Two different layouts of narrow nanoinclusions have been studied in the isobaric-isothermal ensemble. It has been shown that even the narrowest inclusions can significantly alter elastic properties of hard particle crystal by eliminating auxetic properties while maintaining the effective cubic symmetry.

Key words: auxetics, mechanical metamaterials, negative Poisson's ratio, nanochannels, hard sphere crystals, Monte Carlo simulations

I. Introduction

Elastic properties of matter are one of its longest studied aspects. Despite that, studies in materials science still deliver unexpected results that, in turn, drive the technological progress. The discovery of negative Poisson's ratio (PR) [1] materials or, more precisely, showing that they exist in real life [2], providing the first theoretical models, and their solutions for systems with such counterintuitive properties [3, 4], may be considered as an example of such breakthroughs. Since the early 1990's, materials with negative Poisson's ratio are called *auxetics* [5]. Through the past thirty years, they have gained an ever-growing community of researchers dedicated to expanding our understanding of the mechanisms and phenomena behind their properties. These new findings help to solve real-world challenges and advance the applications of auxetic materials [6–9]. The advantage of auxetics is based on the existence of negative Poisson's ratio, at least in some crystallographic directions. In the latter case, they are called *partial auxetics* [10]. The negative Poisson's ra-

tio has been found in model structures [11–15], man-made foams [16, 17], and also in real cubic materials [18], polymers [19, 20], and composites [21]. Apart from the experimental and theoretical [22–24] studies, the computer simulations of auxetics [25–27] are also a rapidly developing source of knowledge on this type of materials. Elastic properties are investigated on various levels, from macroscopic (typically) FEM simulations [28, 29], through mezoscopic models [30], to micro-level, atomic systems [31]. The latter also includes model systems with inclusions [32, 33].

Recent studies have shown that such modifications to the crystal structure of materials exert strong impact on the macroscopic elastic properties and, in particular, the Poisson's ratio [34]. The investigated models with various forms of triple-channel inclusions [34] delivered unexpected conclusions that with a careful choice of the inclusion orientation and layout one can eliminate one of the characteristic features of f.c.c. HS system, namely the negative value of Poisson's ratio in the $[110][1\bar{1}0]$-direction. The effect was observed for various sizes of the inclusions, covering from almost 9 to 19 percent of particles in the system. It has been argued that the layout of inclusions is the crucial parameter behind the observed changes of elastic properties. The present work is a continuation of that research. The goal of this study is to complete the picture by investigating the elastic properties of similar systems featuring very thin inclusions, covering only a little over 2% of particles in the model.

This article has been organized in the following way. The studied models are described in the next section, Sec. II is devoted to the method of elastic properties calculations in the isobaric-isothermal ensemble and the details of computer simulations. The discussion of obtained results is in Sec. IV, whereas Sec. V holds conclusions.

II. The Model

In this work, we consider a model system consisting of N spheres which form the f.c.c. crystal. Particles interact through hard potential, which is expressed as:

$$\phi_{ij} = \begin{cases} \infty, & r_{ij} < \sigma_{ij}, \\ 0\ , & r_{ij} \geq \sigma_{ij}, \end{cases} \tag{1}$$

where r_{ij} is the distance between the centres of particles i and j, $\sigma_{ij} = (\sigma_i + \sigma_j)/2$, σ_i, and σ_j are the diameters of spheres i and j. The *hard sphere* (HS) potential includes short-range correlations originating from the excluded volume effects [35–37], and is one of the fundamental interactions in condensed matter physics [36] and liquid theory [38]. It is the simplest approximation that can exhibit melting and provides an exceptional insight into effects resulting from the relative particle dimensions. From the point of view of the current research, the most important aspect of HS interaction is that it allows one to mimic the existence of the negative Poisson's ratio [34, 39, 40].

Original f.c.c. crystal of spheres with equal diameters (σ) has been modified by replacing arbitrarily selected N_{inc} particles with spheres of another diameter (σ'). The latter particles will be referred to as an inclusion. In the considered model, inclusion is formed by particles lying directly on a selected crystalline axis, which is oriented along one of the main crystalline directions. A single nanochannel is presented in Fig. 1. The selected channel's axis is oriented in the $[010]$-direction, while the red spheres indicate particles forming the inclusion. In this work, inclusions are formed by three nanochannels oriented in the following directions: $[100]$, $[010]$, and $[001]$, thus forming a mutually orthogonal layout. There are many combinations in which such three channels can be arranged in 3D space. Here, as in the previous work [34], we studied two border cases of (i) crossing and (ii) separated nanochannel layout. In Fig. 2, both of them are presented. The illustrated systems have been additionally doubled in each direction. The concentration $c = N_{\text{inc}}/N$ of the included particles depends on the size of the system (N), and also on the particular layout of nanochannels in space.

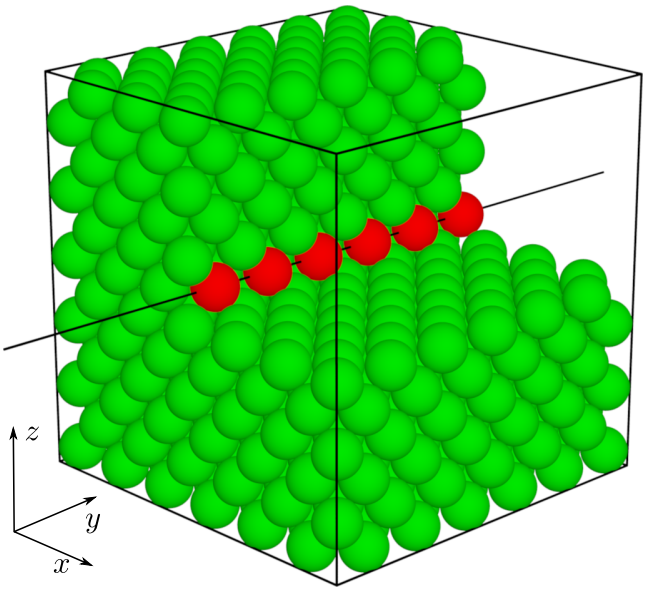

Fig. 1. Illustration of the channel size studied in this work. Inclusion is formed by particles (marked as red spheres) lying directly on a selected crystalline axis marked by the black line. To clearly show channel particles, part of the matrix spheres (green) have been removed from the illustration

Periodic boundary conditions have been applied to all studied models. As it has been stated in previous work [34], results obtained for the periodic box containing the single supercell agreed (within the statistical error) with simulations of systems with the periodic box doubled, quadrupled, and octupled in size. Therefore, to save computational time the systems with the single supercell have been simulated.

III. The Method

III. 1. Theory

To evaluate the elastic properties of the studied systems, extensive Monte Carlo (MC) simulations in the isobaric-isothermal ensemble (NpT) [35, 41] have been performed.

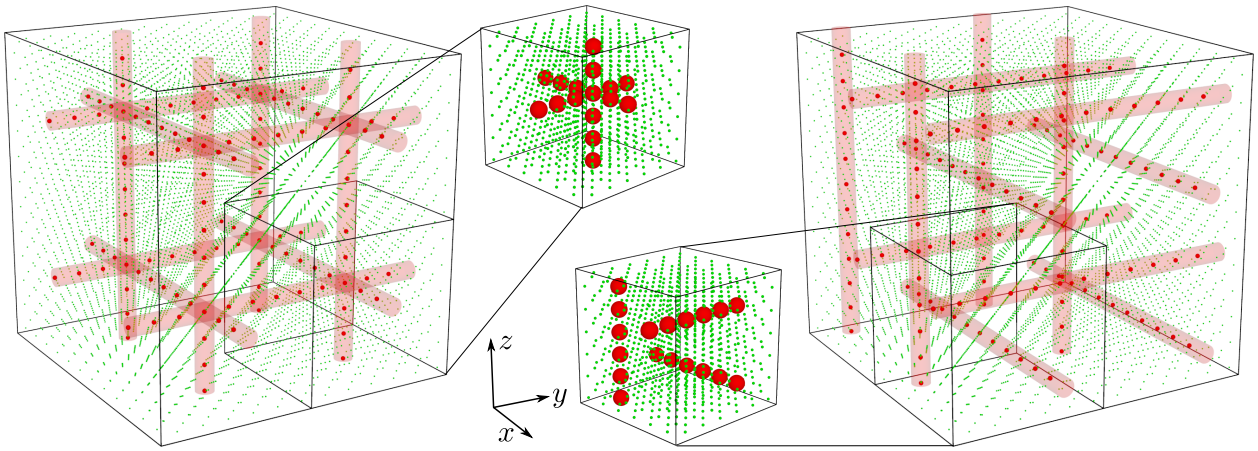

Fig. 2. Different channel layouts illustrated for the system based on a $6 \times 6 \times 6$ f.c.c. supercell, periodically doubled in each direction. The layout with nanochannels crossing each other (left). The layout in which the nanochannels do not contact each other (right). The radii of the nanochannels are less than $\sigma\sqrt{2}/2$ (to include only the particles on the channel's axis). Red spheres represent the channel particles, and the cylindrical shades help to identify the channels' orientation. The green spheres indicating matrix particles have been reduced in size just to reveal the structure of the inclusions

In order to calculate the elastic compliance tensor ($\mathbf{S}$), the Parrinello-Rahman method [42, 43] has been applied. In this method, all $S_{\alpha\beta\gamma\delta}$ elements are easily obtained from shape fluctuations of the periodic box by calculating the strain tensor $\boldsymbol{\varepsilon}$ for the system under dimensionless pressure $p^* = p\sigma^3/k_{\mathrm{B}}T$ as [35, 43]:

$$\boldsymbol{\varepsilon} = \frac{1}{2}\left(\mathbf{h}_p^{-1}.\mathbf{h}.\mathbf{h}.\mathbf{h}_p^{-1} - \mathbf{I}\right), \tag{2}$$

where: k_{B} is the Boltzmann constant, T is the temperature, $\mathbf{I}$ is a unit matrix, $\mathbf{h}$ is a symmetric matrix formed by vectors defining the edges of a periodic parallelepiped, and $\mathbf{h}_p$ is the reference matrix at equilibrium under dimensionless pressure (p^*). The knowledge of the strain tensor components permits determination of the elastic compliance tensor elements as follows [35]:

$$S_{\alpha\beta\gamma\delta} = \frac{V_p}{k_{\mathrm{B}}T}\left\langle \Delta\varepsilon_{\alpha\beta}\Delta\varepsilon_{\gamma\delta}\right\rangle \ , \tag{3}$$

where V_p is the volume of the system at equilibrium under the pressure p^*, $\Delta\varepsilon_{\alpha\beta} = \varepsilon_{\alpha\beta} - \langle\varepsilon_{\alpha\beta}\rangle$, $\langle\varepsilon_{\alpha\beta}\rangle$ is the average in the NpT ensemble, and $\alpha, \beta, \gamma, \delta$ = x, y or z. Based on the knowledge of the elastic compliance tensor, the Poisson's ratio can be calculated by the formula [44]:

$$\nu_{nm} = -\frac{m_\alpha m_\beta S_{\alpha\beta\gamma\delta} n_\gamma n_\delta}{n_\zeta n_\eta S_{\zeta\eta\kappa\lambda} n_\kappa n_\lambda} \ . \tag{4}$$

Poisson's ratio depends on the choice of two directions that are mutually orthogonal. These directions are represented by the unit vector $\vec{\mathbf{n}}$, in which the external stress is applied, and the unit vector $\vec{\mathbf{m}}$, in which the Poisson's ratio is measured. Here, on Greek indexes, the Einstein summation is used. For convenience, further in the text we used the elastic compliance matrix S_{ij} elements in the Voigt notation [45] instead of the $S_{\alpha\beta\gamma\delta}$ tensor elements. The Latin indices for the S_{ij} take the values $i, j = 1, \ldots, 6$.

III. 2. Simulations

The Monte Carlo simulations were performed for systems containing $N = 864$ particles (which corresponds to the supercell of $6 \times 6 \times 6$ f.c.c. cells). The simulations have been carried out in the NpT ensemble at pressures: $p^* = 50$, 100, 250, and 1250. The number of particles forming the inclusion (N_{inc}) varied depending on the layout and was equal to 16 for crossing and 18 for separate nanochannels. This results in concentration of inclusion particles c equal to 1.85% and 2.08%, respectively. Elastic properties of models were studied for different values of inclusion spheres diameters (σ'). They were changed according to the scaling factor σ'/σ, and the values ranged between 0.95 and 1.1 or less (depending on the pressure magnitude). For each value of σ'/σ and p^*, twenty-five independent simulation runs were performed. The length of each run was 10^7 MC cycles with equilibration, which lasted 10^6 MC cycles. For more details on the simulations see ref. [34], and references therein.

IV. Results and Discussion

The problem of the nanochannel layout impacting the elastic properties of the system has been recently investigated. The study showed that three identical channels, but laid out differently in the crystal structure, have a substantially different impact on the system's properties. It was discovered that periodic arrays of orthogonally oriented nanochannels, either crossing each other or remaining separate, contribute to the overall increase of Poisson's ratio and changes in the anisotropy of the models [34]. Two sizes of nanochannels were previously investigated. The overall

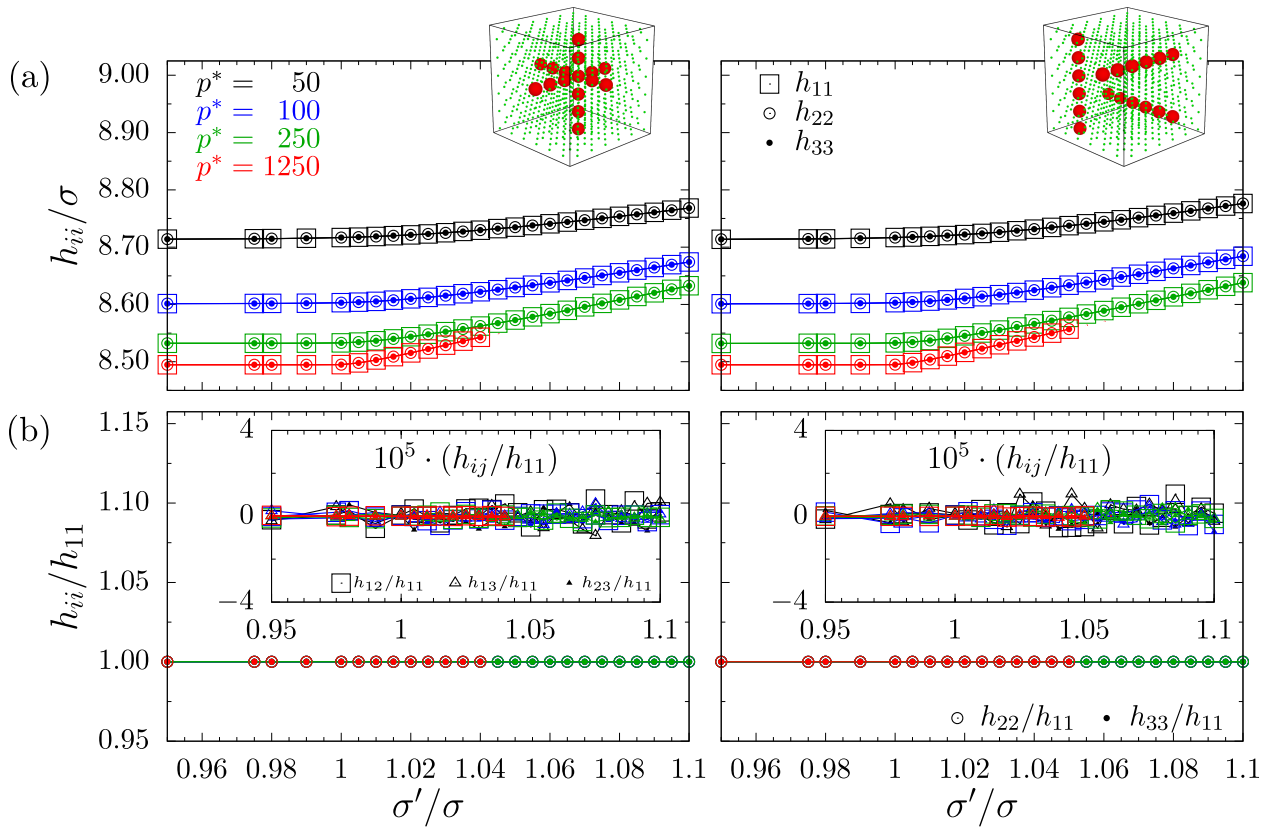

Fig. 3. Components of simulation box matrix (h_{ij}) for all the studied systems presented as a function of the scaling factor σ'/σ. Row (a) contains the diagonal components, whereas row (b) presents h_{22} and h_{33} components divided by h_{11}. The off-diagonal components divided by h_{11} are presented in the inserts to the plots at row (b). Colours indicate data for different values of pressure p^*. In figures at (a) and (b), the computational uncertainties of the presented data are below 0.1% and are much smaller than the symbols representing them. In the inserts in the figures in row (b), the zero value is within the error bars. The miniature structures indicate the corresponding nanochannel layout

concentrations of inclusion particles (depending on the layout) ranged from 8.8% to 18.75%, and consistently showed that the changes in elastic properties are primarily due to the selected layout rather than the size of the nanochannel. The present research is aimed at completing this investigation by studying the systems with the smallest possible inclusion sizes (of c equal to 1.85% and 2.08%) and checking their impact on the Poisson's ratio of the system. The major difference between the current model and the one studied in [34] is that particles forming inclusions do not come in direct contact with each other.

We begin the investigation of very narrow (i) crossing each other and (ii) separate nanochannels by verifying the symmetry of the models studied at four different pressures. Fig. 3 presents the components of box matrix $\mathbf{h}_p$ for systems at equilibrium under the reduced pressure p^*, plotted with respect to the size of the particles forming inclusions (σ'/σ). By convention in this work, the data corresponding to different pressure values (starting from 50 and up to 1250) are marked with different colours indicated on the plots. In row (a) of Fig. 3, the diagonal components of the box matrix are shown. Row (b) presents their relations with respect to the h_{11} component, along with the similar relation for the off-diagonal matrix components (presented on the inserts). The data concerning the different channel layouts have been arranged in columns, indicated by small graphics at the top of the figure. It can be observed that for all the studied cases the diagonal components are equal (within the range of statistical error), and the off-diagonal components are roughly 5 orders of magnitude less than the diagonal ones (and can be treated as equal to zero). This indicates that the shape of the system remains cubic despite the inclusion.

Analysis of the matrices of the elastic compliance ($\mathbf{S}$) or elastic constants ($\mathbf{B}$) allows one to infer the symmetry of studied systems. The elastic compliances are determined by the Monte Carlo simulations from the fluctuations of the shape of periodic box (eq. 3). The elastic constants are calculated from the following relation [35]:

$$\sum_{n,m} S_{ijmn} B_{mnkl} = (\delta_{ik}\delta_{jl} + \delta_{il}\delta_{jk})/2 \,. \qquad (5)$$

In Figs. 4 and 5, the $\mathbf{S}$ and $\mathbf{B}$ are presented in columns for crossing and separate channels, respectively, and for the increasing pressures in descending rows. The following relations between matrix elements: $X_{11} = X_{22} = X_{33}$, $X_{44} = X_{55} = X_{66}$, $X_{12} = X_{13} = X_{23}$ and all the other elements equal to zero were found. Here, X stands for S or B.

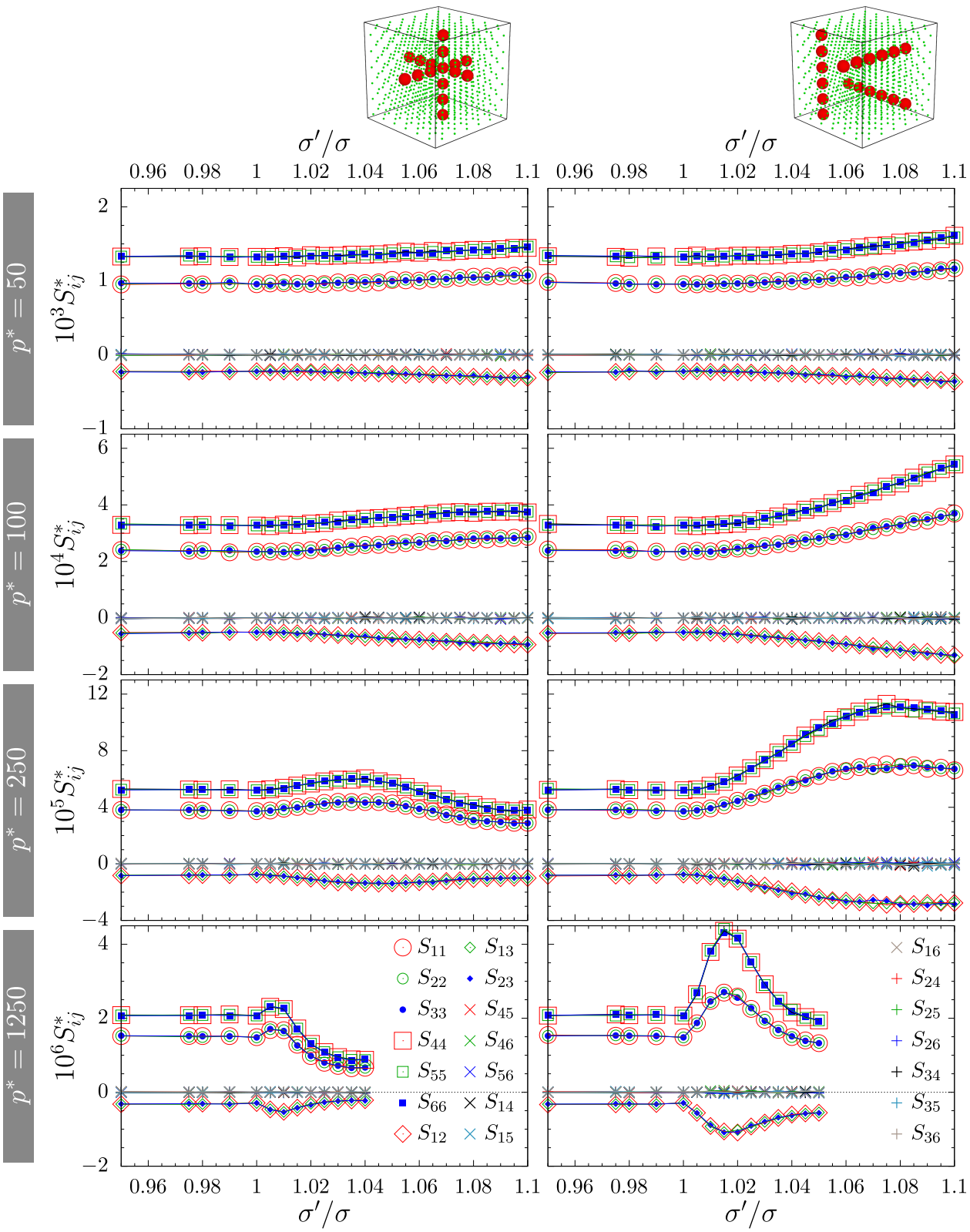

Fig. 4. Components of the elastic compliance matrix **S** for systems with crossing (left column) and separate (right column) nanochannels. Each row corresponds to a different pressure as indicated in the figure. The meaning of the symbols used is explained in the row corresponding to $p^* = 1250$. The computational uncertainties of the presented data are below 3% and are much smaller than the symbols representing them. The quantities represented by the cross ($\times$) and the plus ($+$) symbols are equal to zero within the range of computational error

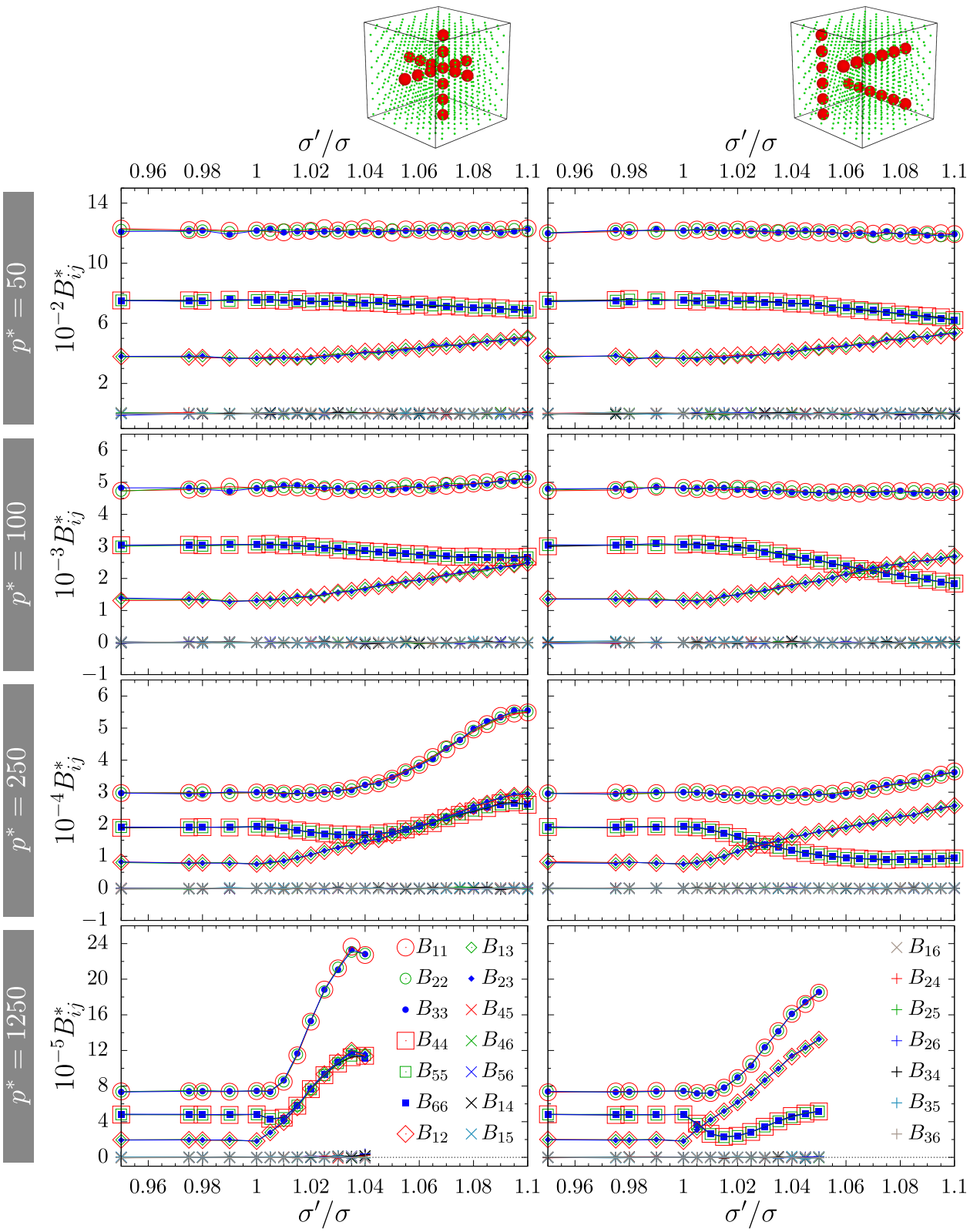

Fig. 5. Components of the elastic constants' matrix $\mathbf{B}$ for systems with crossing (left column) and separate (right column) nanochannels. Each row corresponds to a different pressure as indicated in the figure. The meaning of the symbols used is explained in the row corresponding to $p^* = 1250$. The computational uncertainties of the presented data are below 3% and are much smaller than the symbols representing them. The quantities represented by the cross ($\times$) and the plus ($+$) symbols are equal to zero within the range of computational error

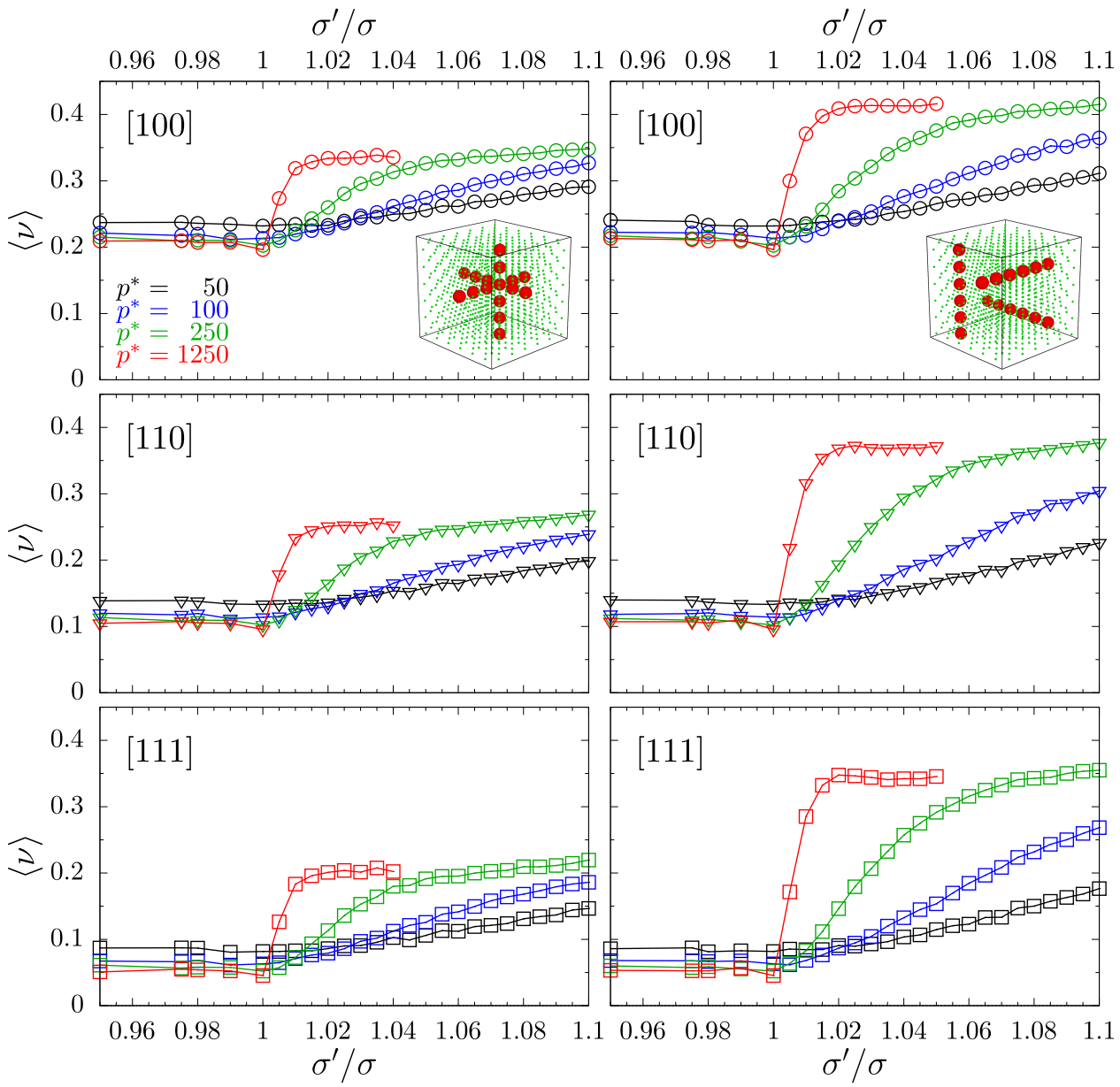

Fig. 6. Averaged Poisson's ratio in main crystallographic directions as a function of the scaling factor σ'/σ. Poisson's ratios in directions [100], [110], and [111] are denoted by circles, triangles, and squares, respectively. As indicated by the added miniature structures, models with crossing nanochannels are presented in the left column, and the right column holds the plots for models with separate nanochannels. Colours indicate data for different values of dimensionless pressure p^*

Those requirements correspond to cubic symmetry. Therefore, one can conclude that all the considered systems show an effective cubic symmetry. *Important remark*: the systems with separate channels and with $\sigma'/\sigma \neq 1$ do not have a 4-fold symmetry axis, so they are not cubic.

In Fig. 4, it can be seen that the impact of the changes in inclusion particle diameters is similar to what was observed earlier for the wider channels [34]. Typically, an increase in σ'/σ ratio is accompanied by an increase of S_{11} and S_{44} compliances, and the decrease of S_{12}. This is regardless of the channel arrangement. The increase, however, is more significant for the separate nanochannels. Along with the increase of the reduced external pressure, it can be observed that the values increase (decrease) only for a certain range of σ'/σ. With further increase of the channel particles size, values for S_{11} and S_{44} start to decline and even fall below the values of cubic system for the $p^* = 1250$ and the crossing channel layout. This is also similar to earlier observations, although the values for corresponding compliances are smaller than in the case of wider channels, especially in reference to the separate nanochannel systems.

Similar observations can be made based on the examination of Fig. 5. The behaviour of elastic constants B_{ij} of investigated systems is qualitatively the same as for the re-

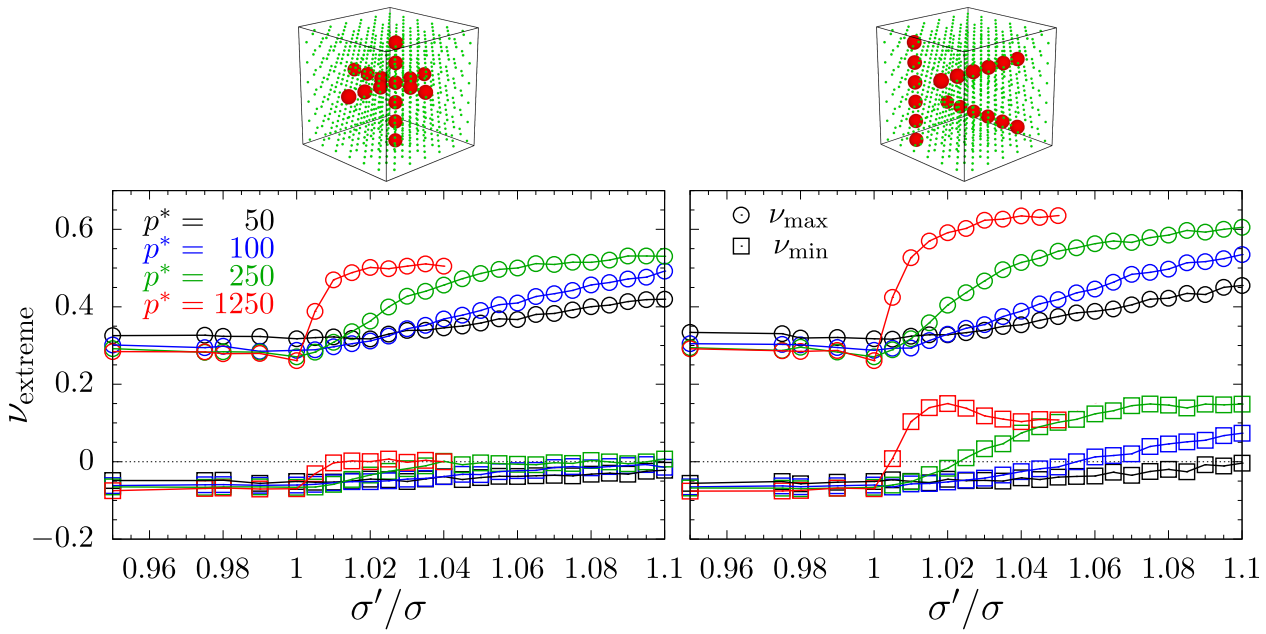

Fig. 7. Extreme Poisson's ratio values for systems, with crossing (left) and separate (right) nanochannels, as a function of the scaling factor σ'/σ. Maximum PR has been marked with circle symbols and square symbols represented the minimum PR. The values of the reduced external pressure p^* have been indicated in colours

spective wider channels. The notable difference is that in the current cases we observe a broader range of stable systems at high pressures. For the low pressure ($p^* = 50$) we can see only little changes to elastic constants when σ'/σ increases. For higher pressures these changes become more significant where the increase of B_{12} and the decrease of B_{44} is clear.

The initial assessment of the impact of inclusions on the Poisson's ratio can be performed by observing its averaged values in the main crystallographic directions [34]. Fig. 6 presents plots organized in columns for the crossing (left) and separate (right) channel layouts. The presented values have been averaged over all possible $\vec{\mathbf{m}}$-directions to the indicated $\vec{\mathbf{n}}$-direction. It can be seen that when $\sigma'/\sigma \neq 1$, the average Poisson's ratios always increases. For both models the increase is more significant for $\sigma'/\sigma > 1$, but one can clearly notice that models with separate inclusions reach higher values of average PR. Higher pressure values make this increase more rapid (occurring for smaller values of σ'/σ). In [100]-direction PR goes above 0.4, which is close to the maximum allowed value of $1/2$ for 3D isotropic systems.

This initial assessment, however, does not provide us with deep insight into the changes in elastic properties of the system. For this reason, we plot the extreme PR values found for any $\vec{\mathbf{n}}$ direction with respect to the σ'/σ ratio. Fig. 7 presents plots for systems with crossing (left column) and separate (right column) nanochannel layouts. The presented data explain the increase of the averaged PR values. Here one can see that the maximum Poisson's ratio increases, especially with an increase of σ'/σ. The difference between the two channel layouts is that while in the case of crossing inclusions the minimum Poisson's ratio increases only slightly, the increase for separate nanochannels is more significant. This explains the stronger increase of averaged PR of models with separate nanochannels. It should also be noted that in the latter models the minimum Poisson's ratio goes above zero. This means that these systems exhibit no auxetic properties. The observations agree with earlier studies where separate layouts of wider nanochannesl removed auxetic properties with an increase of the scaling factor σ'/σ.

Fig. 7 presents only the extreme cases of PR for systems with respect to the σ'/σ value. In the general case, the Poisson's ratio is different for different pairs of $\vec{\mathbf{n}}$ and $\vec{\mathbf{m}}$-directions. Thus, it is difficult to visualize it in the full extent. However, to get more insight one can plot a 3D surface of extreme Poisson's ratios with respect to the $\vec{\mathbf{n}}$-direction described by polar (θ) and azimuthal (φ) angles. All the other PR values for different $\vec{\mathbf{m}}$-directions lie between these two surfaces. Fig. 8 presents the plots for both types of systems under $p^* = 250$ and for selected values of scaling factor σ'/σ, compared to the regular cubic system. The minimum and maximum PR surfaces have been accompanied by the surface of the average PR. It can be noticed that in both systems with inclusions the surface of minimum PR is elevated along with an increase of σ'/σ. In the case of crossing nanochannels at $\sigma'/\sigma = 1.05$, some minor auxetic properties are still present in the system (indicated by the isolines on the $\theta - \varphi$ plane, marking $\nu = 0$), when $\vec{\mathbf{n}}$ is oriented in [110] and corresponding directions. However, in the remaining cases there is no occurrence of PR below zero. The lower parts of the minimum PR surface increase faster for separate nanochannel models, thus decreasing the PR amplitude within the surface itself, but also between the minimum and maximum PR surfaces. This is the reason why the average PR surface tends to flatten. This observation correlates with earlier findings where for wider nanochannels in separate

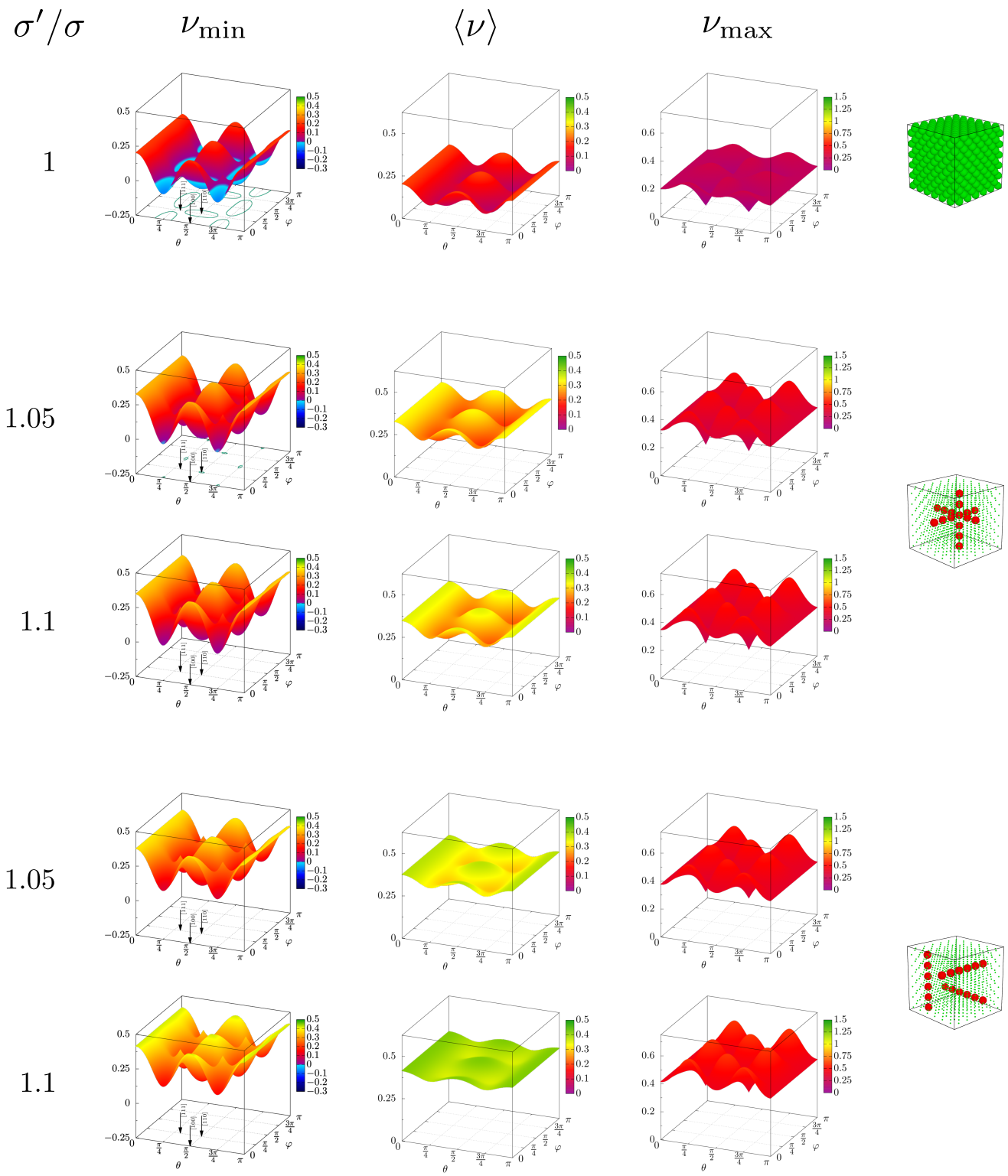

Fig. 8. The surfaces of minimum (bottom row), average (middle row), and maximum (top row) Poisson's ratio, plotted as a function of $\vec{\mathbf{n}}$-direction expressed by θ, φ angles. The plots present cubic system (for reference) and two other values of σ'/σ equal to 1.05 and 1.1 for both channel layouts arranged respectively in columns. The presented data corresponds to systems under $p^* = 250$ reduced external pressure

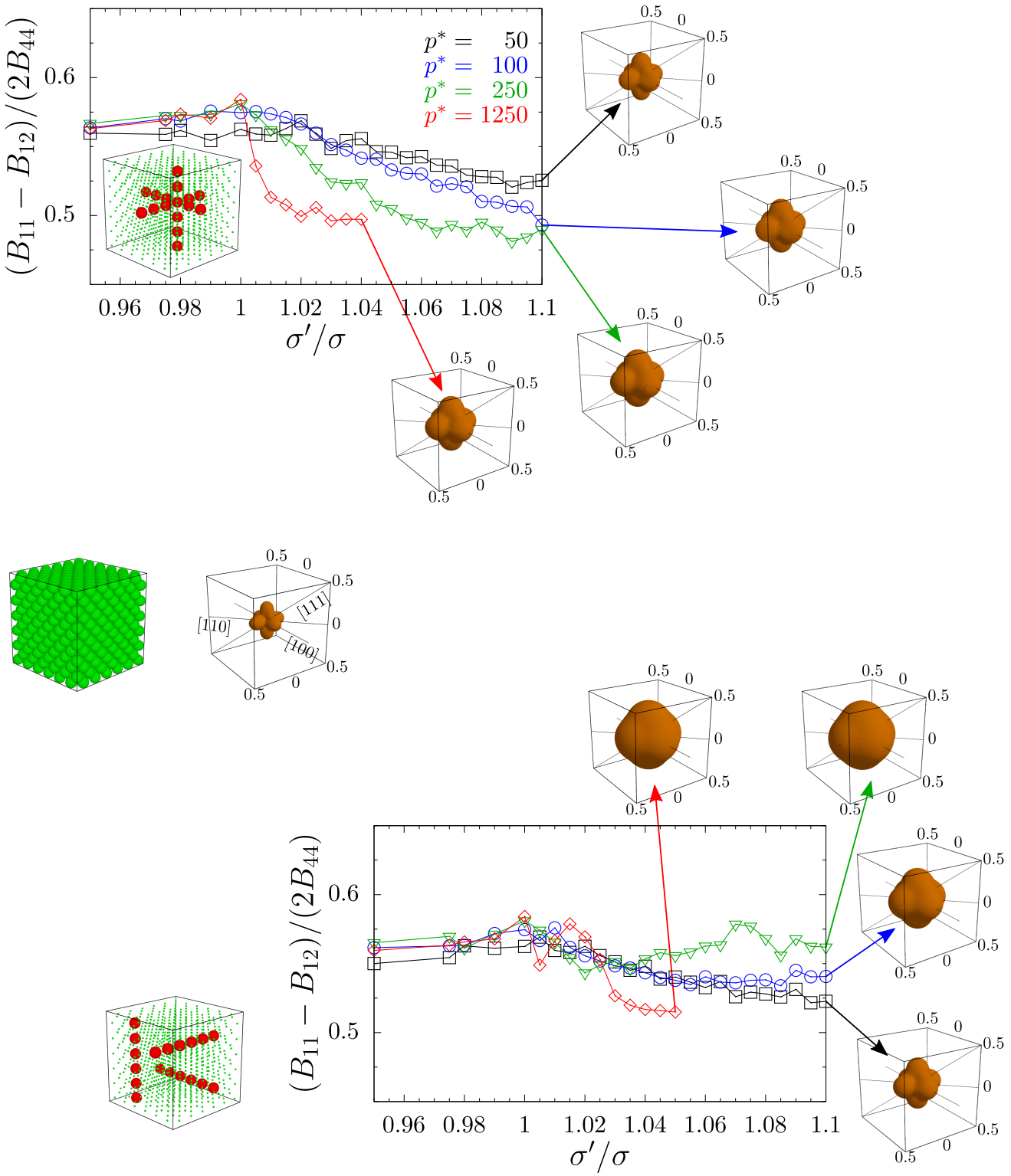

Fig. 9. Calculated relative isotropy criterion (6) for studied systems with crossing and separate nanochannel inclusions (indicated by miniature graphics). The spherical plots of the average Poisson's ratio correspond to systems with σ'/σ indicated by arrow origins. The average PR plotted in top right corner corresponds to regular cubic system at $p^* = 50$

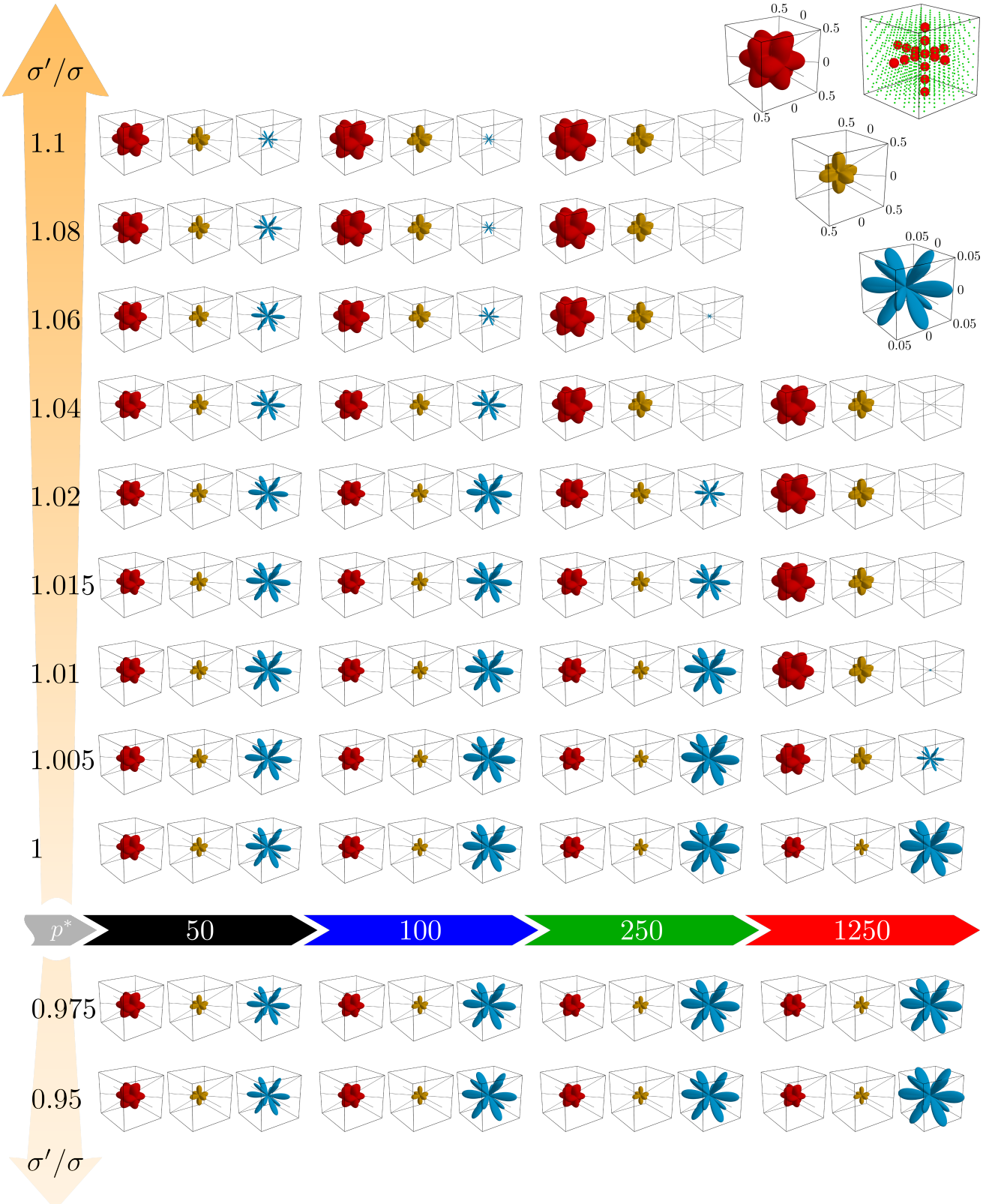

Fig. 10. Poisson's ratios for selected cases of crossing channels model, plotted in spherical coordinate system. The data is presented in the sets of three: maximum PR (red), positive (yellow), and negative part of minimum PR. The arrangement, in the form of array, corresponds to respective pressure and scaling factor values. In the top right corner, examples of each of the three categories have been presented with the exact scale values, which are consistent for all the plots in the figure

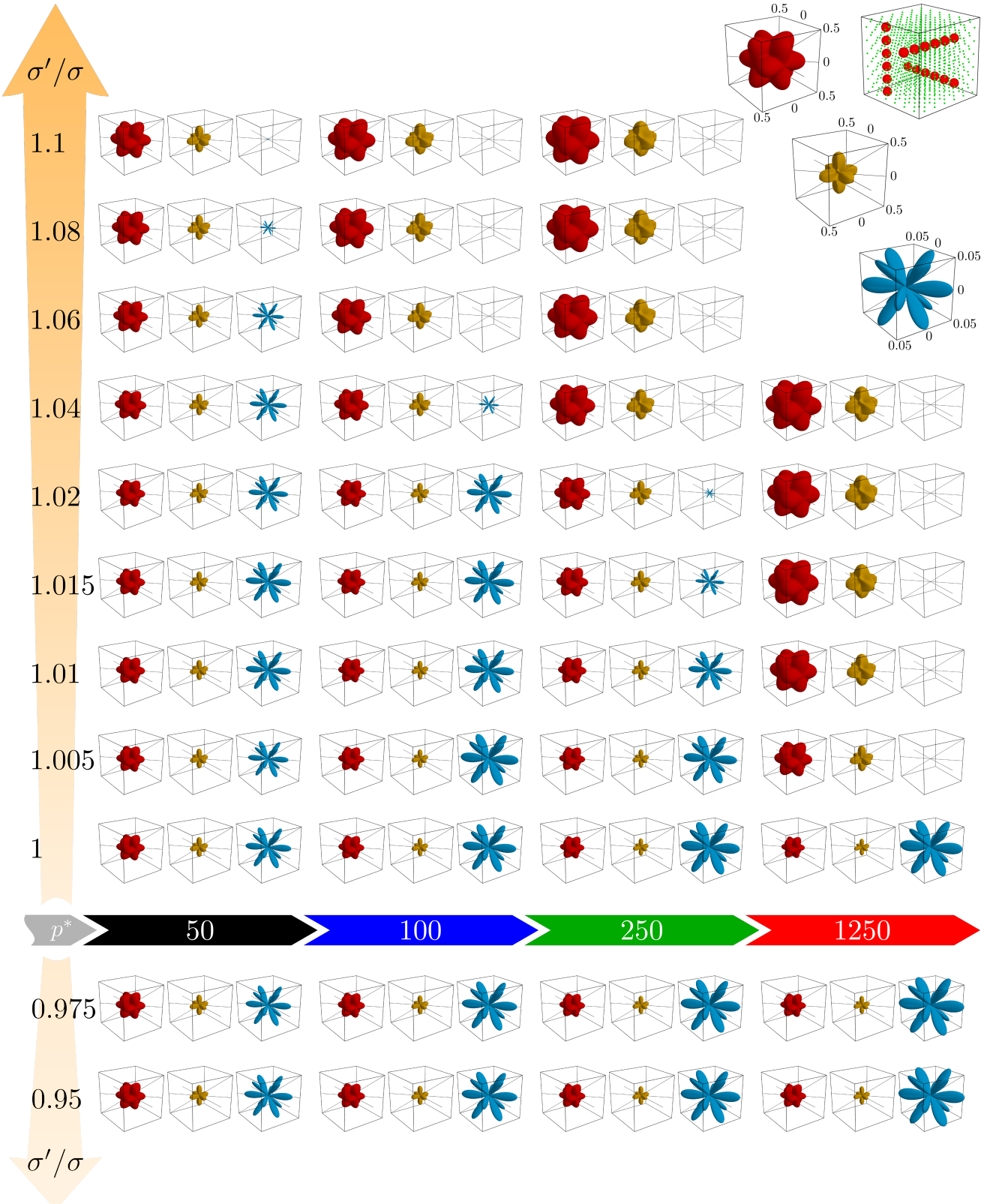

Fig. 11. Poisson's ratios for selected cases of separate channels model, plotted in spherical coordinate system. The data is presented in the sets of three: maximum PR (red), positive (yellow), and negative part of minimum PR. The arrangement, in the form of array, corresponds to respective pressure and scaling factor values. In the top right corner, examples of each of the three categories have been presented with the exact scale values, which are consistent for all the plots in the figure

layout under the same pressure conditions the average PR surface was almost completely flat [34], giving an impression of an effectively elastically isotropic system.

To investigate the changes in the isotropy of the systems at different values of the scaling factor, the criterion for isotropy has been checked:

$$B_{44} = \frac{1}{2}(B_{11} - B_{12}). \tag{6}$$

The results have been presented in Fig. 9, along with plots of average Poisson's ratio surfaces prepared in the spherical coordinate system. It can be seen that the isotropy of the nanochannel systems decreases compared to the cubic one (especially in the case of crossing nanochannels), these changes are not so significant when compared to the ones exerted by wider channels [34]. However, one can see on the spherical plots of the average Poisson's ratio, that at larger pressures for separate nanochannels their shape tends towards a sphere. This is due to the changes observed in Fig. 8.

The plots of the Poisson's ratio in spherical coordinate system (introduced in Fig. 9) constitute a convenient tool to observe the changes in the model, exerted by modifications of external conditions (pressure) or model properties (scaling factor). In Figs. 10 and 11, data for crossing and separate nanochannel systems, respectively, has been presented with respect to pressure and σ'/σ. This large amount of data has been presented in the form of arrays, aligned vertically with respect to the scaling factor and horizontally with respect to pressure. One can observe diminishing auxetic properties and an overall increase of PR values for both systems. This increase is especially visible in the case of separate nanochannel systems where the plots of maximum PR grow substantially, as well as the positive part of minimum PR (yellow), which visually changes shape due to and increase of minimum values significantly above zero.

V. Conclusions

In the present work, the elastic properties of two systems with periodic arrays of orthogonally oriented nanochannels, either crossing each other or separated, have been studied. The results of previous studies showed that (i) similar arrays composed of nanochannels oriented in a single direction enhance auxetic properties [40, 46], and (ii) periodic arrays of three orthogonal nanochannels, crossing or remaining separate, cause the overall increase of Poisson's ratio [34]. Whereas the latter involved inclusions covering at least 8.8% of the system particles, the current study shows that the same effect can be achieved with much smaller inclusions. It has been shown that inclusions containing as low as around 2% of the system particles can exert similar changes to elastic properties of hard sphere crystals. This work confirms that the elastic properties of models can be significantly altered by internal structure modifications, and that the results of the latter are difficult to predict at a macroscopic level.

Acknowledgment

This work was supported by grant No. 2017/27/B/ST3/02955 of the National Science Centre, Poland. The computations were partially performed at Poznań Supercomputing and Networking Center (PCSS).

References

[1] L.D. Landau, E.M. Lifshitz, *Theory of Elasticity*, London, UK, Pergamon Press (1986).

[2] R.S. Lakes, *Foam structures with a negative Poisson's ratio*, Science **235**, 1038–1040 (1987).

[3] K.W. Wojciechowski, *Constant thermodynamic tension Monte Carlo studies of elastic properties of a two-dimensional system of hard cyclic hexamers*, Mol. Phys. **61**, 1247–1258 (1987).

[4] K.W. Wojciechowski, *Two-dimensional isotropic model with a negative Poisson ratio*, Phys. Lett. A, **137**, 60–64 (1989).

[5] K.E. Evans, *Auxetic polymers: a new range of materials*, Endeavour **15**, 170–174 (1991).

[6] L. Mizzi, D. Attard, A. Casha, J.N. Grima, R. Gatt, *On the suitability of hexagonal honeycombs as stent geometries*, Phys. Status Solidi B **251**, 328–337 (2014).

[7] X. Ren, J. Shen, T. Phuong, T. Ngo, Y.M. Xie, *Auxetic nail: Design and experimental study*, Comp. Struct. **184**, 288–298 (2018).

[8] Y.-C. Wang, H.-W. Lai, J.X. Ren, *Enhanced auxetic and viscoelastic properties of filled reentrant honeycomb*, Phys. Status Solidi B **257**(10), 1900184 (2020).

[9] X.Y. Zhang, X. Ren, *A simple methodology to generate metamaterials and structures with negative Poisson's ratio*, Phys. Status Solidi B **257**(10), 2000439 (2020).

[10] A.C. Brańka, D.M. Heyes, K.W. Wojciechowski, *Auxeticity of cubic materials under pressure*, Phys. Status Solidi B **248**, 96–104 (2011).

[11] R.S. Lakes, *Advances in negative Poisson's ratio materials*, Adv. Mater. **5**, 293–296 (1993).

[12] K.E. Evans, A. Alderson, *Auxetic materials: Functional materials and structures from lateral thinking!*, Adv. Mater. **12**, 617–628 (2000).

[13] R. Lakes, *Negative-Poisson's-ratio materials: Auxetic solids*, Annual Review of Materials Research **47**, 63–81 (2017).

[14] T.-C. Lim, *Mechanics of Metamaterials with Negative Parameters*, Springer, Singapore (2020).

[15] K.K. Dudek, R. Gatt, M.R. Dudek, J.N. Grima, *Controllable hierarchical mechanical metamaterials guided by the hinge design*, Materials **14**(4), 758 (2021).

[16] O. Duncan, A. Alderson, T. Allen, *Fabrication, characterization and analytical modeling of gradient auxetic closed cell foams*, Smart Mater. Struct. **30**(3), 035014 (2021).

[17] T. Allen, T. Hewage, C. Newton-Mann, W. Wang, O. Duncan, A. Alderson, *Fabrication of auxetic foam sheets for sports applications*, Phys. Status Solidi B **254**(12), 700596 (2017).

[18] R.H. Baughman, J.M. Shacklette, A.A. Zakhidov, S. Stafstrom, *Negative Poisson's ratios as a common feature of cubic metals*, Nature **392**, 362–365 (1998).

[19] D.Y. Fozdar, P. Soman, J.W. Lee, L.H. Han, S.C. Chen, *Three-dimensional polymer constructs exhibiting a tunable negative Poisson's ratio*, Adv. Funct. Mater. **21**, 2712–2720 (2011).

[20] K. Alderson, S. Nazaré, A. Alderson, *Large-scale extrusion of auxetic polypropylene fibre*, Phys. Status Solidi B **253**(7), 1279–1287 (2016).

[21] K.L. Alderson, V.R. Simkins, V.L. Coenen, P.J. Davies, A.Alderson, K.E. Evans, *How to make auxetic fibre reinforced composites*, Phys. Status Solidi B **242**(3), 509–518 (2005).
[22] D.T. Ho, H. Kim, S.-Y. Kwon, S.Y. Kim, *Auxeticity of face-centered cubic metal (001) nanoplates*, Phys. Status Solidi B **252**(7), 1492–1501 (2015).
[23] R.V. Goldstein, V.A. Gorodtsov, D.S. Lisovenko, M.A. Volkov, *Two-layered tubes from cubic crystals: Auxetic tubes*, Phys. Status Solidi B **254**(12), 1600815 (2017).
[24] V.A. Gorodtsov, M.A. Volkov, D.S. Lisovenko, *Out-of-plane tension of thin two-layered plates of cubic crystals*, Phys. Status Solidi B **258**(12), 2100184, (2021).
[25] D.T. Ho, S. Park, S. Kwon, T. Han, S.Y. Kim, *Negative Poisson's ratio in cubic materials along principal directions*, Phys. Status Solidi B **253**(7), 1288–1294 (2016).
[26] D.S. Lisovenko, J.A. Baimova, L.K. Rysaeva, V.A. Gorodtsov, A.I. Rudskoy, S.V. Dmitriev, *Equilibrium diamond-like carbon nanostructures with cubic anisotropy: Elastic properties*, Phys. Status Solidi B **253**(7), 1295–1302 (2016).
[27] J.N. Grima-Cornish, L. Vella-Żarb, K.W. Wojciechowski, J.N. Grima, *Shearing deformations of β-cristobalite-like boron arsenate*, Symmetry **13**, 977 (2021).
[28] A.A. Pozniak, K.W. Wojciechowski, J.N. Grima, L. Mizzi, *Planar auxeticity from elliptic inclusions*, Composites Part B **94**, 379–388 (2016).
[29] T. Strek, J. Michalski, H. Jopek, *Computational analysis of the mechanical impedance of the sandwich beam with auxetic metal foam core*, Phys. Status Solidi B **256**(1), 1800423 (2019).
[30] W.G. Hoover, C.G. Hoover, *Searching for auxetics with DYNA3D and ParaDyn*, Phys. Status Solidi B **242**(3), 585–594 (2005).
[31] K.V. Tretiakov, P.M. Piglowski, K. Hyzorek, K.W. Wojciechowski, *Enhanced auxeticity in Yukawa systems due to introduction of nanochannels in [001]-direction*, Smart Mater. Struct. **25**, 054007 (2016).
[32] E. Pasternak, I. Shufrin, A.V. Dyskin, *Thermal stresses in hybrid materials with auxetic inclusions*, Comp. Struct. **138**, 313–321 (2016).
[33] D.T. Ho, C.T. Nguyen, S.Y. Kwon, S.Y. Kim, *Auxeticity in metals and periodic metallic porous structures induced by elastic instabilities*, Phys. Status Solidi B **256**, 1800122 (2018).
[34] J.W. Narojczyk, M. Bilski, J.N. Grima, P. Kedziora, D. Morozow, M. Rucki, K.W. Wojciechowski, *Removing auxetic properties in f.c.c. hard sphere crystals by orthogonal nanochannels with hard spheres of another diameter*, Materials **15**, 1134 (2022).
[35] K.W. Wojciechowski, K.V. Tretiakov, M. Kowalik, *Elastic properties of dense solid phases of hard cyclic pentamers and heptamers in two dimensions*, Phys. Rev. E **67**, 036121 (2003).
[36] D. Frenkel, *Order through entropy*, Nature Materials **14**, 9–12 (2015).
[37] K.V. Tretiakov, K.W. Wojciechowski, *Auxetic, partially auxetic, and nonauxetic behaviour in 2D crystals of hard cyclic tetramers*, Phys. Status Solidi RRL **14**, 2000198 (2020).
[38] J.P. Hansen, I.R. McDonald, *Theory of Simple Liquids*, Academic Press, Amsterdam, The Netherlands (2006).
[39] K.V. Tretiakov, K.W. Wojciechowski, *Poisson's ratio of the fcc hard sphere crystal at high densities*, J. Chem. Phys. **123**, 074509 (2005).
[40] J.W. Narojczyk, K.W. Wojciechowski, K.V. Tretiakov, J. Smardzewski, F. Scarpa, P.M. Piglowski, M. Kowalik, A.R. Imre, M. Bilski, *Auxetic properties of a f.c.c. crystal of hard spheres with an array of $[001]$-nanochannels filled by hard spheres of another diameter*, Phys. Status Solidi B **256**, 1800611 (2019).
[41] K.W. Wojciechowski, A.C. Brańka, *Negative Poisson ratio in a two-dimensional isotropic solid*, Phys. Rev. A **40**, 7222–7225 (1989).
[42] M. Parrinello, A. Rahman, *Polymorphic transitions in single crystals: A new molecular dynamics method*, J. Appl. Phys. **52**, 7182–7190 (1981).
[43] M. Parrinello, A. Rahman, *Strain fluctuations and elastic constants*, J. Chem. Phys. **76**, 2662–2666 (1982).
[44] S.P. Tokmakova, *Stereographic projections of Poisson's ratio in auxetic crystals*, Phys. Status Solidi B **242**(3), 721–729 (2005).
[45] J.F. Nye, *Physical Properties of Crystals, Their Representation by Tensors and Matrices*, Oxford, UK, Clarendon Press (1957).
[46] K.V. Tretiakov, P.M. Piglowski, J.W. Narojczyk, K.W. Wojciechowski, *Selective enhancement of auxeticity through changing a diameter of nanochannels in Yukawa systems*, Smart Mater. Struct. **27**, 115021 (2018).

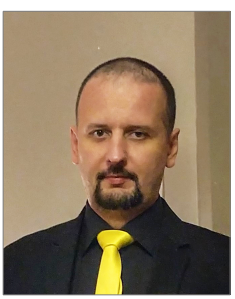

Jakub W. Narojczyk received his PhD from the Institute of Molecular Physics of the Polish Academy of Sciences in Poznań (IMP PAS). He is a computational physicist with a strong background in Monte Carlo and Molecular Dynamics simulation methods. He has in-depth knowledge of C programming language and a solid experience in administration of GNU/Linux class operating systems as well as High-Performance Computing environment. He works as an Assistant Professor in the IMP PAS, where he conducts research (by means of computer simulations) on elastic properties of model materials, with emphasis on their Poisson's ratio. The research is aimed at the search for systems for which the Poisson's ratio takes negative values (such materials are called auxetics) as well as mechanisms and phenomena responsible for the decrease of the Poisson's ratio of materials. Currently, his studies are focused on the influence of various forms of nanoinclusions in the atomic structure on the elastic properties of various model systems. He guest co-edited one special issue of Physica Status Solidi B and four abstract books from the conferences on Auxetics and Related Systems. He is a peer reviewer for various scientific journals including Applied Physics Letters, Applied Sciences, Advanced Theory and Simulations, Carbon, Materials and Design, Physica Status Solidi B, and Computational Methods in Science and Technology.

Konstantin V. Tretiakov graduated summa cum laude in Industrial Electronics from the The Pavel Sukhoi State Technical University (Gomel, Belarus) in 1994. He received his PhD degree in Physics from the Institute of Molecular Physics, Polish Academy of Sciences (Poznan, Poland) in 2000 supervised by Prof. Krzysztof W. Wojciechowski. In 2002-2004, Dr. Tretiakov was a Postdoctoral Fellow (with Prof. S. Scandolo) in the Condensed Matter and Statististical Physics Section at the Abdus Salam International Center for Theoretical Physics (Trieste, Italy). In 2007-2009, Dr. Tretiakov worked with Prof. Bartosz Grzybowski in the Department of Chemical and Biological Engineering at Northwestern University (Evanston IL, USA). He prepared habilitation in 2011 and since 2014 he is Associate Professor of the Department of Computational Physics of Complex Systems in Institute of Molecular Physics, Polish Academy of Sciences. Dr. habil. Tretiakov specializes in statistical physics and computer simulation of many body systems, with research focusing on non-equilibrium self-assembling systems, transport properties of soft-matter, and elastic properties of solids, in particular materials exhibiting negative Poisson's ratio.

Krzysztof W. Wojciechowski is a Full Professor and Head of the Division of Soft Matter Physics and Functional Materials as well as the Group of Computational Physics of Complex Systems at the Institute of Molecular Physics of the Polish Academy of Sciences (IMP PAS) in Poznań. He is also a Full Professor at the President Stanisław Wojciechowski University in Kalisz. He received the MSc degree in Theoretical Physics and the MSc degree in Mathematics from the Adam Mickiewicz University in Poznan. He earned the PhD in Physics from the IMP PAS, where he also habilitated. His research interests concern, among other topics, statistical-mechanics of hard-body systems, algorithms for simulations of many-body systems, auxetics and influence of various mechanisms on the Poisson's ratio of condensed matter systems, materials with unstable inclusions, generators of (pseudo)random numbers, applications of fractional derivative in physics, and exotic liquid crystalline phases. He is an author and co-author of more than 200 research papers written in English, Polish or Russian and published in such journals as Phys. Rev. Lett., Advanced Materials, Phys. Lett. A, Phys. Rev. A, Phys. Rev. B, Phys. Rev. E, J. Chem. Phys., J. Phys. Chem. A, Molecular Physics, etc. Prof. Wojciechowski guest co-edited more than two dozen thematic issues (on auxetics and related materials, mechanics of continuous media, statistical mechanics of condensed matter, computer simulation methods, nonlinear and disordered systems) for international journals including Phys. Status Solidi B (14), J. Non-Cryst. Solids (4), Smart Materials and Structures (2), J. Mech. Mat. Struct. (2), Rev. Adv. Mat. Sci. (2), etc. He is a member of the Editorial Board of the CMST and TASK Quarterly.